Juan Du
H. Milton Stewart School of Industrial and Systems Engineering,
Georgia Institute of Technology,
Atlanta, GA 30332
e-mail: juan.du@isye.gatech.edu

Xiaowei Yue
Mem. ASME
Grado Department of Industrial and Systems Engineering,
Virginia Polytechnic Institute and State University,
Blacksburg, VA 24061
e-mail: xwy@vt.edu

Jeffrey H. Hunt
The Boeing Company,
900 N Sepulveda Blvd, El Segundo, CA 90245
e-mail: jeffrey.h.hunt@boeing.com

Jianjun Shi[1]
Fellow ASME
H. Milton Stewart School of Industrial and Systems Engineering,
Georgia Institute of Technology,
Atlanta, GA 30332
e-mail: jianjun.shi@isye.gatech.edu

Optimal Placement of Actuators Via Sparse Learning for Composite Fuselage Shape Control

Shape control is a critical task in the composite fuselage assembly process due to the dimensional variabilities of incoming fuselages. To realize fuselage shape adjustment, actuators are used to pull or push several points on a fuselage. Given a fixed number of actuators, the locations of actuators on a fuselage will impact on the effectiveness of shape control. Thus, it is important to determine the optimal placement of actuators in the fuselage shape control problem. In current practice, the actuators are placed with equal distance along the edge of a fuselage without considering its incoming dimensional shape. Such practice has two limitations: (1) it is non-optimal and (2) larger actuator forces may be applied for some locations than needed. This paper proposes an optimal actuator placement methodology for efficient composite fuselage shape control by developing a sparse learning model and corresponding parameter estimation algorithm. The case study shows that our proposed method achieves the optimal actuator placement for shape adjustments of the composite fuselage. [DOI: 10.1115/1.4044249]

Keywords: actuator placement, composite fuselage, shape control, sparse learning, ADMM, assembly, control and automation, inspection and quality control

1 Introduction

Composite materials have been widely used in the aerospace industry due to its superior characteristics such as high strength-to-weight ratio and low life-cycle cost. Currently, some major structures of an airplane are made of composite materials, which comprise more than 50% composites by weight [1]. In practice, there are dimensional errors in the fabrication of a fuselage due to the complexity of the composite part manufacturing [2]. As a result, shape control has become a common practice in the composite fuselage assembly process.

In this paper, the dimensional deviations between the real manufactured shape and the design shape of a fuselage are denoted by the initial shape distortions; the magnitude of shape adjustment is denoted by the shape correction; and the dimensional deviations between the shape after control and the design shape of a fuselage are denoted as the adjusted shape deviations. A placement is an arrangement of actuators' locations on a fuselage. In addition, a composite fuselage is called fuselage for short.

In order to achieve shape control of a fuselage, a number of actuators are needed to pull or push several points of the fuselage to change its shape distortions [3,4]. Figure 1(*a*) shows a feasible 10-actuator placement strategy with equal distance between two adjacent actuators. Figure 1(*b*) shows corresponding shape adjustment by these actuators. In the coordinate system (Fig. 1(*b*)), the original point is the center of the edge circle; the *X*–*Y* plane is defined as the intermediate horizontal plane with *X*-axis aligned with the longitudinal axis of the fuselage, and the *Z*-axis is perpendicular to the *X*–*Y* plane. After the shape adjustment by these actuators, the shape correction can be obtained. In this paper, we focus on the measurement points that are close to the edge plane of the fuselage, as shown in Fig. 1(*c*). In current practice, the actuators are placed in equal distance between two adjacent actuators, which does not consider the initial shape distortions of the incoming fuselage. This fixed actuator placement strategy has two limitations: (1) it is non-optimal. The shape of the fuselage after adjustment under the fixed placement of actuators may not be optimal for a specific incoming fuselage. In other words, there is no guarantee that the optimal shape control can be realized by a fixed actuator placement for different incoming fuselages. (2) It may provide larger stress and strains than needed. Since the fixed placement may not be optimal, larger actuator forces may be applied for some locations during shape control than it needs to be. In consequence, the stress and strain are large, which may potentially damage the fuselage. Hence, an efficient actuator placement method is needed to apply smaller, but sufficient forces to achieve better performance in the fuselage shape control.

Developing an efficient and optimal actuator placement method is a challenging task due to the following reasons: (1) The initial shape distortions of fuselages vary from one fuselage to another, and the optimal actuator placement should adapt to the different initial shape distortions. It is challenging to propose an optimal placement of actuators that works for each fuselage. (2) Multiple actuators and fixtures are applied to a fuselage, and the shape of the fuselage after adjustment cannot be directly derived from the mechanics due to the compliant and anisotropic property of complex composite structures. Instead of theoretical derivation, approximation such as the finite element analysis (FEA) method can be used to calculate the deformation after applying the forces. However, the FEA simulation is time-consuming and only available for a given, specific actuator placement. It is not feasible to run many simulations for finding the optimal actuator placement in practice. (3) To prevent the potential damage of a fuselage during shape control, the forces applied from each actuator cannot exceed the maximum force (MF) limits allowed. Under the same amount of shape correction, smaller actuator forces are preferred. Thus, how to place actuators efficiently given the force limits is challenging.

To overcome these three challenges, we propose an optimal actuator placement method for fuselage shape control. First, we develop a model to link shape corrections with actuator forces. Then, we propose a constrained sparse learning model to minimize the weighted mean square of adjusted shape deviations (WMSDs), so

[1]Corresponding author.

Manuscript received August 19, 2018; final manuscript received June 1, 2019; published online July 31, 2019. Assoc. Editor: Dragan Djurdjanovic.

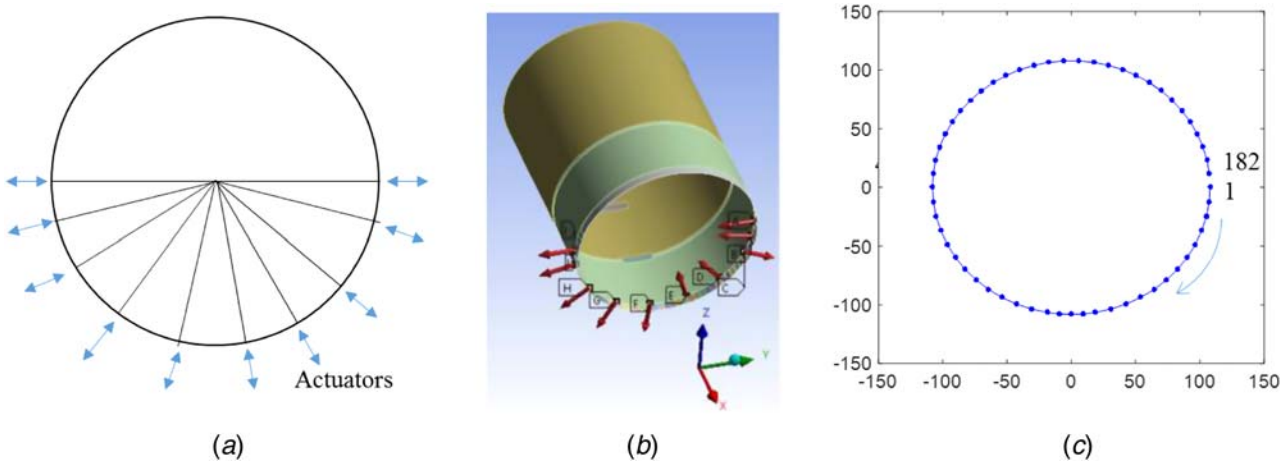

Fig. 1 Illustrations for a fuselage shape control: (*a*) a feasible actuator placement, (*b*) a schematic drawing of shape adjustment, and (c) layout of measurement points

as to obtain the optimal actuator placement for a given number of actuators. Last, we develop an efficient algorithm to estimate parameters of the proposed model by integrating the binary search algorithm and the Alternating Direction Method of Multipliers (ADMM) algorithm.

The remainder of this paper is organized as follows. Section 2 provides a literature review of the topics on actuator placement for shape control. Then, Sec. 3 develops a sparse learning model and the associated parameter estimation algorithm. A case study is provided to validate the performance of our proposed method in Sec. 4. Finally, Sec. 5 concludes this paper.

2 Literature Review

In literature, various methods of placing actuators for large structure shape control have been developed. These methods can be classified into two categories.

The first category contains the actuator or sensor placements for smart structures. In literature, differential equations and input control energy were derived to achieve the optimal actuator placement. This type of methods works well for dynamic systems and piezoelectric actuators [5,6] but does not work for fuselage shape control. The reason is that it is not feasible to obtain differential equations of composite fuselages due to their compliant and nonlinear properties.

The other category is the optimal actuator placement for the static shape control. First, we briefly introduce this category from the modeling perspective. An analytical investigation of shape control for beam structure was provided by Haftka and Adelman [7]. To analyze the correction of the initial shape distortions from a statistical perspective, Burdisso and Haftka [8] further considered two techniques: an adjoint technique and modal expansion. All these optimal actuator placement methods are based on the objective function of minimizing the WMSD after shape control. For some engineering problems where the worst shape distortion among the critical points after shape control is the focus. Hakim and Fuchs [9] formulated the objective function of the optimal actuator placement as minimizing the worst-case distortion. However, all aforementioned studies focused on the beam-based structures, such as beams, trusses, and reflectors. Compared to the beam-based structure, the fuselage structure is more complicated. The analytical derivation is infeasible for the fuselage in mechanics. In addition, the fuselage is made by the composite materials, which is compliant and anisotropic. Thus, these methods cannot be used directly for fuselage shape control. To address this limitation, we propose a sparse learning model to link shape deviations with actuator forces, and the structural parameters can be obtained from the surrogate modeling.

Next, we briefly introduce the optimal actuator placement for the static shape control from the estimation algorithm perspective. Haftka and Adelman [10] proposed the optimal placement of actuators for shape control by formulating a discrete optimization problem and developing a heuristic integer programming algorithm. However, this method cannot guarantee the global optimum. To overcome the computation issue of discrete optimization, Burdisso and Haftka [11] proposed a continuum approximation to reduce computational costs. Ponslet et al. [12], Jiao and Djurdjanovic [13] applied the genetic algorithm to deal with the combinatorial optimization problem to further improve the optimization performance. A genetic algorithm has a high probability to obtain the solution near the global optimum but it is computationally expensive. To address this issue, Furuya and Haftka [14] proposed a procedure that evaluated the effectiveness of the possible locations and discarded ineffective ones to reduce the computation cost. Jiao and Djurdjanovic [15] further proposed to apply a reactive tabu search for large-scale combinatorial optimization problem in the multistage manufacturing process. However, all these methods cannot guarantee the global optimum due to the approximation of the discrete optimization problem. To address this limitation, our proposed estimation algorithm can efficiently achieve the global optimum due to the convexity of the proposed sparse learning model.

For fuselage shape control, Wen et al. [3] developed a new shape control system and conducted the feasibility analysis by using the FEA. They assumed that the actuators were uniformly distributed on the edge of the outer surface of the lower semi-fuselage. Based on this FEA platform, Yue et al. [4] proposed a surrogate model to establish the relationship between the shape correction and actuator forces applied to the fuselage. By minimizing the WMSD, they could calculate the optimal forces applied by each actuator for fuselage shape control and then assembly [16]. However, as they only considered the uniform actuator layout for all different incoming fuselages, shape control performance may not be optimal for a specific fuselage due to its special initial shape distortions.

To address this problem, this paper proposes an optimal actuator placement method for fuselage shape control, which considers the initial shape distortions. Given all the feasible locations of actuators, we propose a sparse learning model to link actuator forces with the WMSD of the fuselage. To estimate the model parameters efficiently, we develop an algorithm that integrates the binary search and the ADMM algorithm. After obtaining the optimal actuator placement, the optimal forces can be obtained by minimizing the WMSD.

3 Sparse Learning-Based Methodology for Optimal Placement of Actuators

3.1 Problem Definition and Formulation. Let n denote the number of measurement points of shape deviations of a fuselage, and m denote the number of feasible positions (e.g., candidate positions where an actuator may be placed) for actuators in the fuselage edge plane. We assume that the mechanical response behavior of the fuselage to the actuator forces is linear, which indicates the shape correction of each measurement point in the fuselage can be calculated by a linear combination of shape corrections under each actuator force. This assumption can be physically interpreted from the elastic deformation in mechanics. Hence, the adjusted shape deviations can be formulated as

$$\boldsymbol{\delta} = \boldsymbol{\psi} + \boldsymbol{UF} \tag{1}$$

where $\boldsymbol{\psi} \in R^n$ represents the initial shape distortions at n measurement points. $\boldsymbol{U} \in R^{n\times m}$ is the displacement matrix where the element $\boldsymbol{U}_{ij}$ corresponds to the shape correction of measurement point i given a unit of force at location j. $\boldsymbol{F} \in R^m$ is the force vector where the element $\boldsymbol{F}_j$ is the force of actuator at location j. $\boldsymbol{\delta} \in R^n$ is the adjusted shape deviation vector, where the element $\boldsymbol{\delta}_i$ represents the adjusted shape deviations of the measurement point i. In this paper, we adopt that the actuators are used to minimize the WMSD of fuselages, i.e., δ^2_{wmsd}, which is defined as

$$\delta^2_{wmsd} = \boldsymbol{\delta}' \boldsymbol{B} \boldsymbol{\delta} \tag{2}$$

where $\boldsymbol{\delta}'$ is the transpose of $\boldsymbol{\delta}$. $\boldsymbol{B} \in R^{n\times n}$ is a diagonal weighted matrix, which represents the importance of different measurement points. Note m is the number of all feasible locations for actuators, and M is the number of actuators for fuselage shape control. We aim to select M locations from m feasible ones, which indicates that only M components of the vector $\boldsymbol{F}$ are nonzero. Therefore, this problem can be formulated as

$$\begin{aligned} &\min_{F} \ \delta^2_{wmsd} = (\boldsymbol{\psi} + \boldsymbol{UF})' \boldsymbol{B} (\boldsymbol{\psi} + \boldsymbol{UF}) \\ &\text{s.t.} \ \ ||\boldsymbol{F}||_0 = M, \ \ \boldsymbol{F}_L \preceq \boldsymbol{F} \preceq \boldsymbol{F}_Q \end{aligned} \tag{3}$$

Here, $\preceq$ is the component-wise inequality. $\boldsymbol{F}_L$ and $\boldsymbol{F}_Q$ are the lower bound and upper bound of actuator forces, respectively. $\|\cdot\|_0$ is the l_0 norm, which counts the number of nonzero entries in a vector. The l_0 norm function is non-convex, non-smooth, discontinuous, and globally non-differentiable.

Finding the sparse solution of the optimization problem (3) is NP-hard [17] and even difficult to approximate [18]. Donoho [19] showed that for most underdetermined systems, the sparse solution could be found by solving a convex optimization problem when a sufficiently sparse solution exists. He pointed out that the solution of minimizing l_1 norm was also the sparsest solution. Hence, we transform the optimization problem (3) into a convex optimization with a l_1 norm:

$$\begin{aligned} &\min_{F} \ L(\boldsymbol{F}) = (\boldsymbol{\psi} + \boldsymbol{UF})' \boldsymbol{B} (\boldsymbol{\psi} + \boldsymbol{UF}) + \lambda ||\boldsymbol{F}||_1 \\ &\text{s.t.} \ \ \boldsymbol{F}_L \preceq \boldsymbol{F} \preceq \boldsymbol{F}_Q \end{aligned} \tag{4}$$

where λ is a tuning parameter, and its value is selected to meet the requirement of $\|\boldsymbol{F}\|_0 = M$.

There are two key differences between our model and the current literature [6–12]: (1) The current literature only considered selecting M actuators from m feasible locations and formulated the problem as an integer programming problem. However, this problem formulation tends to be computationally costly when m is large. In comparison, we propose a sparse and convex representation of the problem, which can be solved efficiently, as to be discussed in Sec. 3.2. (2) The current literature obtained the displacement matrix $\boldsymbol{U}_0 \in R^{n\times M}$ from mechanics. The analytical derivation of the matrix $\boldsymbol{U}_0$ is limited to simple structures such as beams. For complex structures, matrix $\boldsymbol{U}_0$ needs to be obtained from the FEA. This indicates that once one of the M actuator locations is changed, the FEA should be conducted again to obtain $\boldsymbol{U}_0$ before the optimization, which is computationally expensive and time-consuming. Here, we propose a displacement matrix $\boldsymbol{U} \in R^{n\times m}$ under all feasible m locations, and we obtain this $\boldsymbol{U}$ matrix from a surrogate model.

Since the deformation of measurement points in the shape control should be elastic [20], we use a linear model [21] as the surrogate model, which is formulated as

$$\boldsymbol{Y}_i = \boldsymbol{F}_D \boldsymbol{\beta}_i + \boldsymbol{\varepsilon}_i \tag{5}$$

where $\boldsymbol{F}_D \in R^{N\times m}$ and $\boldsymbol{Y}_i \in R^N$ are the design force matrix and shape correction vector of the measurement point i, $i = 1, 2, \ldots, n$. $\boldsymbol{F}_D$ and $\boldsymbol{Y}_i$ are obtained from the design of experiment (DOE). N is the sample size of DOE and $\boldsymbol{\varepsilon}_i$ is the noise vector that follows a Gaussian distribution. $\boldsymbol{\beta}_i \in R^{m\times 1}$ is the coefficient vector for measurement point i, which can be estimated by the least-squares method. The displacement matrix is $\boldsymbol{U} = [\boldsymbol{\beta}_1, \ \boldsymbol{\beta}_2, \ldots, \ \boldsymbol{\beta}_n]'$. More details about surrogate modeling can be found in Ref. [4]. Figure 2 shows the schematic diagram of the proposed method. It is worth noting that the main focus of this paper is to propose a sparse learning methodology for actuator placement optimization.

3.2 Algorithm for Parameter Estimation. Since there are non-smooth term $\|\boldsymbol{F}\|_1$ and linear constraints in the optimization problem (4), the conventional convex optimization algorithm [22], such as the interior point method, cannot be implemented efficiently. The alternating direction method of multipliers (ADMM) [23] is widely used to solve the optimization problem that features a separable objective. The optimization problem (4) has the objective function that can be separated into the summations of $(\boldsymbol{\psi} + \boldsymbol{UF})' \boldsymbol{B} (\boldsymbol{\psi} + \boldsymbol{UF})$ and $\lambda \|\boldsymbol{F}\|_1$, so we apply the ADMM algorithm to solve the optimization problem (4).

We can reformulate the optimization problem (4) as

$$\begin{aligned} &\text{minimize} \ f(\boldsymbol{F}) + \lambda ||z||_1 \\ &\text{s.t.,} \ \ \boldsymbol{F} - z = 0 \end{aligned} \tag{6}$$

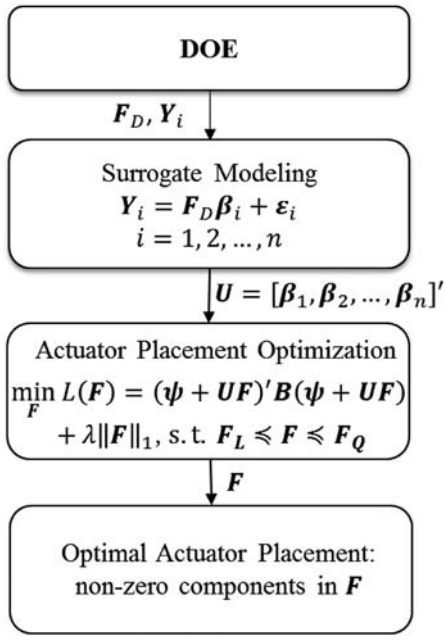

Fig. 2 Schematic diagram of our proposed method

where $\boldsymbol{F} \in R^m$, $z \in R^m$, and $f(\boldsymbol{F}) = \chi_C + (\boldsymbol{\psi} + \boldsymbol{UF})'\boldsymbol{B}(\boldsymbol{\psi} + \boldsymbol{UF})$. χ_C is an indicator function of the constraint set $C = \{\boldsymbol{F} \in R^m: \ \boldsymbol{F}_L \preceq \boldsymbol{F} \preceq \boldsymbol{F}_Q\}$, i.e.,

$$\chi_C = \begin{cases} \infty & \boldsymbol{F} \notin C \\ 0 & \boldsymbol{F} \in C \end{cases} \tag{7}$$

Let $g(z) = \lambda \|z\|_1$, the augmented Lagrangian of the optimization problem (6) is

$$L_\rho = f(\boldsymbol{F}) + g(z) + \boldsymbol{y}'(\boldsymbol{F} - z) + \frac{\rho}{2}||\boldsymbol{F} - z||_2^2 \tag{8}$$

where ρ is the augmented Lagrangian parameter and y is the dual variable. According to Ref. [23], the ADMM can be expressed as

$$\boldsymbol{F}^{k+1} := \underset{\boldsymbol{F}}{\operatorname{argmin}}\left(f(\boldsymbol{F}) + \frac{\rho}{2}||\boldsymbol{F} - \boldsymbol{z}^k + \boldsymbol{u}^k||_2^2\right) \tag{9}$$

$$\boldsymbol{z}^{k+1} := \underset{z}{\operatorname{argmin}}\left(g(z) + \frac{\rho}{2}||\boldsymbol{F}^{k+1} - z + \boldsymbol{u}^k||_2^2\right) \tag{10}$$

$$\boldsymbol{u}^{k+1} := \boldsymbol{u}^k + \boldsymbol{F}^{k+1} - \boldsymbol{z}^{k+1} \tag{11}$$

where $\boldsymbol{u} = \mathbf{y}/\rho$ is the scaled dual variable. In Proposition 1, we can derive the main steps of the ADMM for the optimization problem (4) according to formulas (9–11).

Proposition 1. *Given the formulation (6) and formulas (9–11), the scaled form of the ADMM of the optimization problem (4) can be derived as*

$$\boldsymbol{F}^{k+1} := \prod\nolimits_C((2\boldsymbol{U}'\boldsymbol{BU} + \rho\boldsymbol{I})^{-1}(\rho\boldsymbol{z}^k - \rho\boldsymbol{u}^k - 2\boldsymbol{U}'\boldsymbol{B}\boldsymbol{\psi})) \tag{12}$$

$$\boldsymbol{z}^{k+1} := S_{\lambda/\rho}(\boldsymbol{F}^{k+1} + \boldsymbol{u}^k) \tag{13}$$

$$\boldsymbol{u}^{k+1} := \boldsymbol{u}^k + \boldsymbol{F}^{k+1} - \boldsymbol{z}^{k+1} \tag{14}$$

Here, $\boldsymbol{I} \in R^{m\times m}$ is an identity matrix. $\prod_C$ is a Euclidean projection onto the convex set $C = \{\boldsymbol{F} \in R^m: \ \boldsymbol{F}_L \preceq \boldsymbol{F} \preceq \boldsymbol{F}_Q\}$, which can be denoted as

$$\prod\nolimits_C(v) = \underset{\boldsymbol{F}\in C}{\operatorname{argmin}}(||\boldsymbol{F} - \boldsymbol{v}||_2) \tag{15}$$

$S_{\lambda/\rho}$ is the soft thresholding operator of $\|\cdot\|_1$, which is

$$S_{\lambda/\rho}(v) = (v - \lambda/\rho)_+ \ \ (-v - \lambda/\rho)_+ \tag{16}$$

where $(x)_+$ is short for max $\{x, 0\}$.

The proof of Proposition 1 is provided in Appendix A.

According to Ref. [23], the convergence of the ADMM is guaranteed in our context, which means that we can obtain the global optimum of the optimization problem (4) via the ADMM. In practice, Boyd et al. [23] suggested that a reasonable termination of the ADMM is that both the primal and dual residuals should be small, i.e.,

$$||\boldsymbol{r}^k||_2 \le e_1, \ \text{and} \ ||\boldsymbol{s}^k||_2 \le e_2 \tag{17}$$

where $\boldsymbol{r}^k = \boldsymbol{F}^k - \boldsymbol{z}^k$ is the primal residual and $\boldsymbol{s}^k = -\rho(\boldsymbol{z}^k - \boldsymbol{z}^{k-1})$ is the dual residual. $e_1 > 0$ and $e_2 > 0$ are the tolerances, which can be chosen by using an absolute criterion and a relative criterion, i.e.,

$$e_1 = \sqrt{m}e_3 + e_4 \max\{||\boldsymbol{z}^k||_2, \ ||\boldsymbol{F}^k||_2\} \tag{18}$$

$$e_2 = \sqrt{m}e_3 + e_4\rho||\boldsymbol{u}^k||_2 \tag{19}$$

where $e_3 > 0$ and $e_4 > 0$ are an absolute tolerance and a relative tolerance, respectively. Algorithm 1 shows the proposed ADMM algorithm.

Algorithm 1 The ADMM for estimating

(1) **Input**: parameter ρ, λ, e_3, e_4, m, $\boldsymbol{B}$, $\boldsymbol{U}$, $\boldsymbol{\psi}$
(2) **Initialize** $\boldsymbol{F}^0$, z^0, $\boldsymbol{u}^0$
(3) Repeat
(4) $\quad \boldsymbol{F}^{k+1} = \prod_C((2\boldsymbol{U}'\boldsymbol{BU} + \rho\boldsymbol{I})^{-1}(\rho\boldsymbol{z}^k - \rho\boldsymbol{u}^k - 2\boldsymbol{U}'\boldsymbol{B}\boldsymbol{\psi}))$
(5) $\quad \boldsymbol{z}^{k+1} = S_{\lambda/\rho}(\boldsymbol{F}^{k+1} + \boldsymbol{u}^k)$
(6) $\quad \boldsymbol{u}^{k+1} = \boldsymbol{u}^k + \boldsymbol{F}^{k+1} - \boldsymbol{z}^{k+1}$.
(7) $\quad \boldsymbol{r}^{k+1} = \boldsymbol{F}^{k+1} - \boldsymbol{z}^{k+1}$
(8) $\quad \boldsymbol{s}^{k+1} = \rho(\boldsymbol{z}^{k+1} - \boldsymbol{z}^k)$
(9) $\quad e_1 = \sqrt{m}e_3 + e_4 \max\{\|\boldsymbol{z}^{k+1}\|_2, \|\boldsymbol{F}^{k+1}\|_2\}$
(10) $\quad e_2 = \sqrt{m}e_3 + e_4||\rho\boldsymbol{u}^{k+1}||_2$
(11) **Until** $\|\boldsymbol{r}^{k+1}\|_2 \le e_1$, and $\|\boldsymbol{s}^{k+1}\|_2 \le e_2$ or $k = K$

In Algorithm 1, K is the maximum number of iterations. The tuning parameter λ in model (4) is used to control the sparsity of $\boldsymbol{F}$, i.e., the number of nonzero components in vector $\boldsymbol{F}$. For the required number M of actuators, the number of nonzero components in the vector $\boldsymbol{F}$ is M. Hence, we need to search the value of λ such that $\|\boldsymbol{F}\|_0 = M$. The binary search algorithm is one of the most important search algorithms for finding a value in a linear array by ruling out half of the values at each step, which is the case of our context. Hence, we propose to use the binary search algorithm for estimating λ. To perform the binary search algorithm, the range of parameter λ needs to be determined. The minimum value of λ is zero, which indicates no shrinkage of vector $\boldsymbol{F}$. The maximum value of λ is provided in Proposition 2 that penalizes all the components of vector $\boldsymbol{F}$ into zero.

Proposition 2. *The maximum value of λ for the binary search is $\lambda_{\max} = \|2\boldsymbol{U}'\boldsymbol{B}\boldsymbol{\psi}\|_\infty$.*

The derivation of Proposition 2 is provided in Appendix B. Notably, for searching λ such that $\|\boldsymbol{F}\|_0 = M$, $M > 0$, there is no need to search the value larger than $\lambda_{\max}$, which is the minimum value of λ to penalize all the components of vector $\boldsymbol{F}$ into zero. The binary search algorithm for determining λ is listed in Algorithm 2.

Algorithm 2 A binary search algorithm for estimating λ

(1) **Input**: parameter ρ, e_3, e_4, M, m, $\boldsymbol{B}$, $\boldsymbol{U}$, $\boldsymbol{\psi}$
(2) **Initialize** $\lambda_{\min} = 0$, $\lambda_{\max} = \|2\boldsymbol{U}'\boldsymbol{B}\boldsymbol{\psi}\|_\infty$
(3) Repeat
(4) $\quad \lambda = (\lambda_{\min} + \lambda_{\max})/2$
(5) $\quad$ Calculate $\boldsymbol{F}$ from Algorithm 1
(6) $\quad$ If $\|\boldsymbol{F}\|_0 = M$
(7) $\quad\quad$ Stop
(8) $\quad$ Else if $\|\boldsymbol{F}\|_0 < M$
(9) $\quad\quad \lambda_{\max} = \lambda$
(10) $\quad$ Else
(11) $\quad\quad \lambda_{\min} = \lambda$
(12) $\quad$ End
(13) **End**

According to the Algorithm 2, we can obtain λ^* such that $\|\boldsymbol{F}\|_0 = M$. The locations of nonzero components of vector $\boldsymbol{F}$ indicate the locations of actuators. To adjust the shape of the fuselage, the applied force $\boldsymbol{F}_c$ of actuators in these locations aims to minimize adjusted shape deviations, i.e.,

$$\min_{\boldsymbol{F}_c} \ L(\boldsymbol{F}_c) = (\boldsymbol{\psi} + \boldsymbol{U}_c\boldsymbol{F}_c)'\boldsymbol{B}(\boldsymbol{\psi} + \boldsymbol{U}_c\boldsymbol{F}_c), \ \text{s.t.} \quad \boldsymbol{F}_L \preceq \boldsymbol{F}_c \preceq \boldsymbol{F}_Q \tag{20}$$

where $\boldsymbol{U}_c \in R^{n\times M}$ is the submatrix of $\boldsymbol{U} \in R^{n\times m}$, which corresponds to M locations of nonzero components of vector $\boldsymbol{F}$. Equation (20) is a conventional constrained quadratic programming problem, which is convex, continuous, smooth, and globally differentiable. Hence, we follow Yue et al. [4] and use the interior point method to solve this problem.

In practice, due to the material property of composite structures, the elements of displacement matrix are usually very small. To avoid the numerical implementation issues, such as floating-point errors [24], we multiply a large constant number L_N of the objective function $(\boldsymbol{\psi}+\boldsymbol{UF})'\boldsymbol{B}(\boldsymbol{\psi}+\boldsymbol{UF})$ in the optimization problem (4), which does not have influences on the optimal solution. In this way, the numerical problem induced by $\boldsymbol{U}$ matrix can be avoided in real implementations.

4 Case Study

An FEA model is useful to mimic the manufacturing system, especially when the manufacturing data is scarce and precious. In this case study, we use an FEA model to generate the data and validate the proposed methodology. This model has been validated with the experimental data [3,4]. In our case study, we assume that there are $m=18$ feasible actuator locations uniformly distributed from -12 deg to 192 deg, as shown in Fig. 3. Notably, all those 18 feasible locations of actuators are placed at the lower part of the fuselage for ease of engineering implementation. $M=10$ locations are selected from all those 18 feasible locations for fuselage shape control. The number of measurement points is $n=182$, and we take the same importance of each measurement point, i.e., $B=diag(1/n)$.

4.1 Design of Experiment and Surrogate Modeling. To mimic the initial shape distortions of fuselages and obtain displacement matrix $\boldsymbol{U}$, we use the Maximin Latin Hypercube Design [25] to generate 40 training samples and 20 testing samples. The forces are sampled in the range from -200 lb to 200 lb by $m=18$ actuators, and the initial shape distortions are shown in Fig. 4. The maximum initial shape distortion is 3.422 in., which commendably emulate the real case.

In our case study, we first use the training samples to estimate parameters in the surrogate model (5) and then use the testing samples to test the surrogate model performance. Figure 5 shows the training error and the testing error of the surrogate model. The *Y*-axis shows the root mean square error (RMSE). The mean values of the RMSEs of training data and testing data are 1.86×10^{-5} in. and 1.92×10^{-5} in., respectively, thereby indicating the proposed surrogate model has a very good prediction capability.

4.2 Actuator Placement and Static Shape Control Result. In this section, we evaluate our proposed method based on 20 testing samples. The parameters in Algorithm 2 are set as $\rho=1$, $e_3=10^{-4}$, $e_4=10^{-2}$, and $K=1000$, which are regular settings of the ADMM algorithm. $L_N=10^7$ is set to avoid the numerical computation issues. In our problem, the ADMM converges quickly and only takes less than 0.5 s to obtain the optimal solution for one sample in MATLAB R2014B by a computer with Intel Core-i5-4200U @ 2.30 GHz processor, 8 GB of RAM. The computational speed meets the requirements for fuselage shape control. In Fig. 6, we randomly select several samples and show the proposed actuator locations. The circular curves are the ideal shape, and the shaded area is

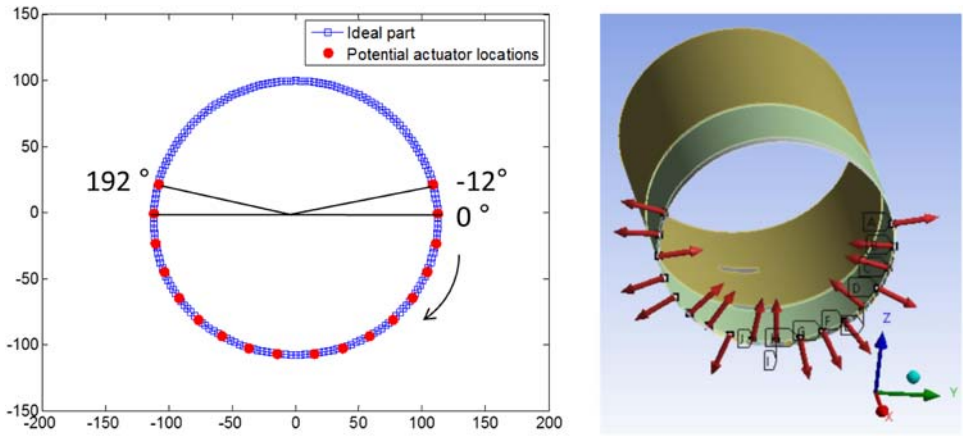

Fig. 3 $m=18$ number of feasible actuator locations

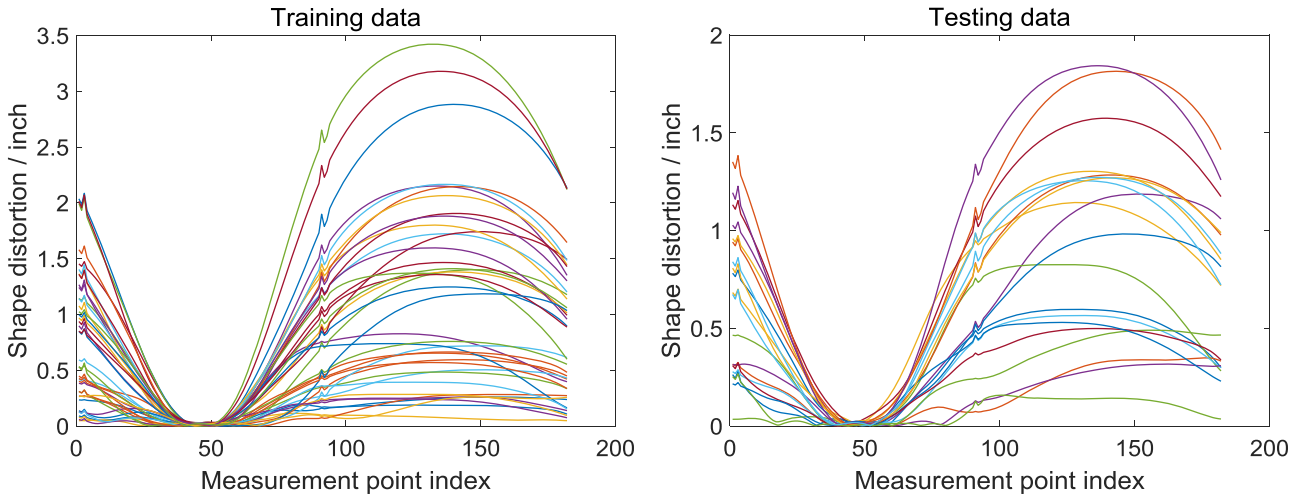

Fig. 4 The initial shape distortions generated by FEA

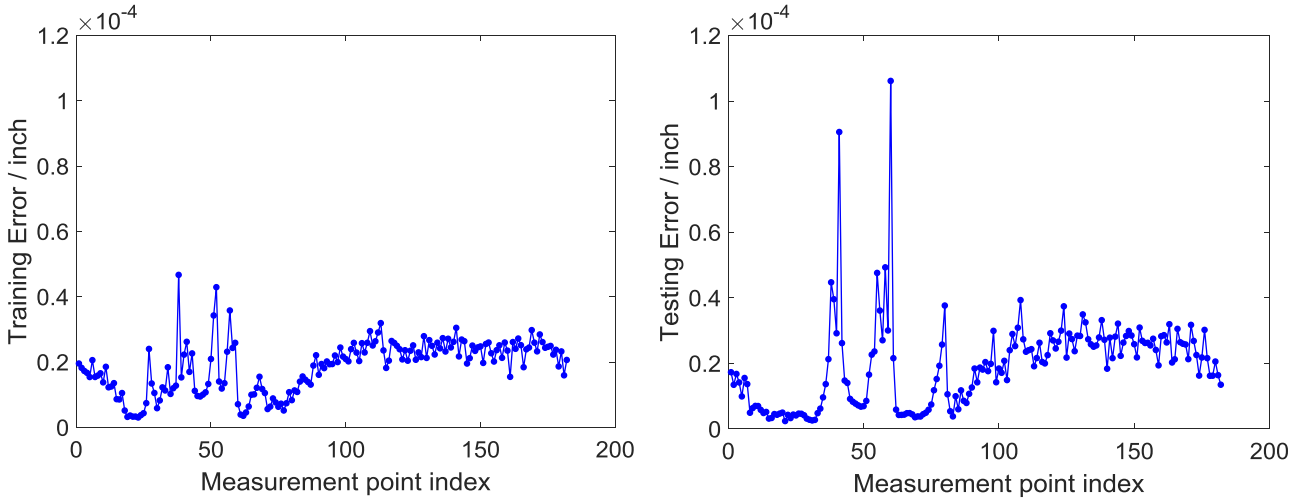

Fig. 5 The training error and the testing error of the surrogate model

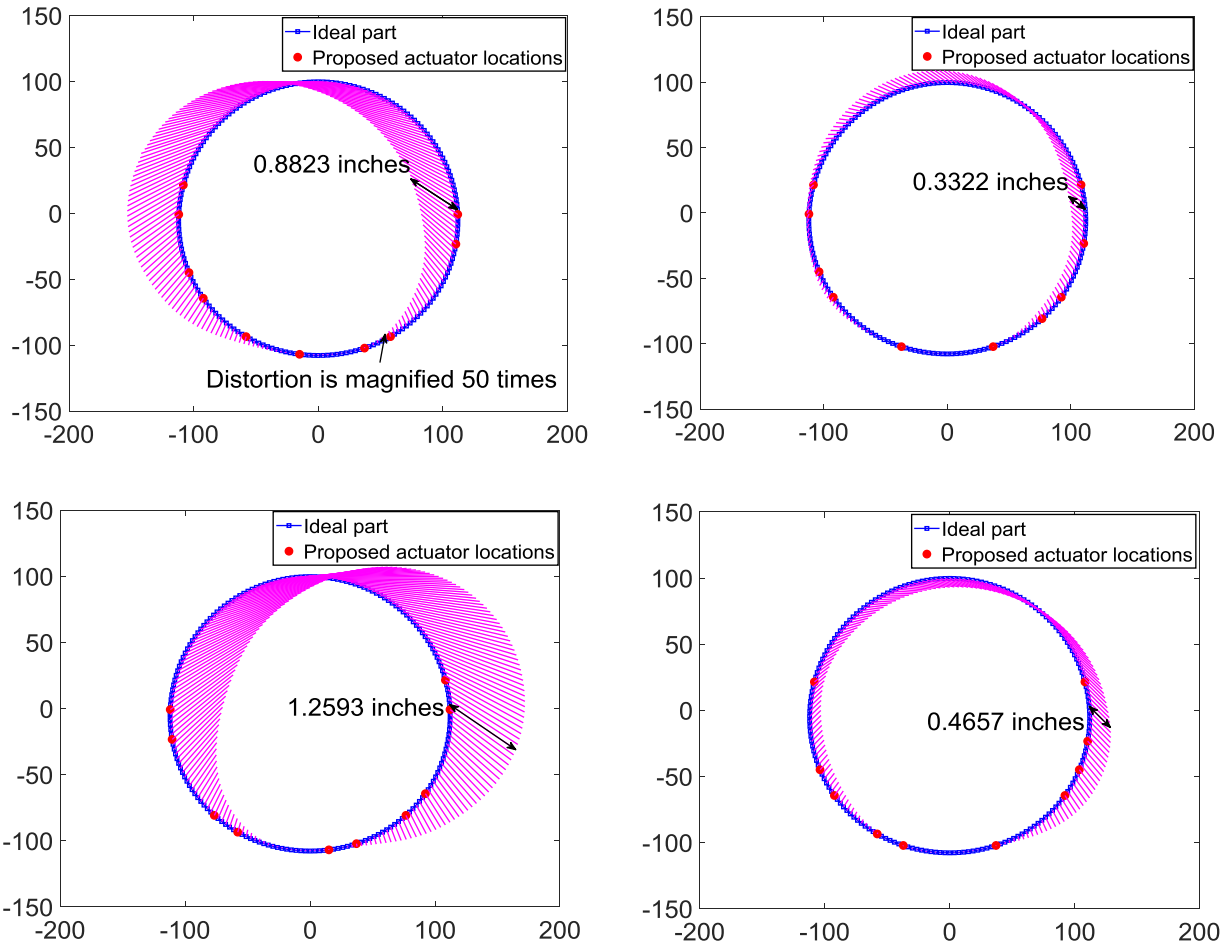

Fig. 6 The proposed actuator placements according to different initial shape distortions

the initial shape distortions generated from the FEA. To show it clearly, we magnify the distortions 50 times, and the true initial shape distortion magnitude of one measurement point is marked. Ten round points are also marked on the shape curve, which are the actuator locations selected by our proposed method. Figure 6 shows that our proposed method selects different actuator locations according to different initial shape distortions of fuselages. Our method tends to distribute more actuators in the locations with larger initial shape distortions, which is consistent with the engineering intuition.

We introduce three quantitative indices to evaluate the performance of our method, which are the maximum of adjusted shape deviations (MD), the root mean square of adjusted shape deviations (RMSD), and the maximum force (MF) for shape control. Because the practitioners currently use a fixed placement to adjust the fuselage shape with different initial shape distortions, we compare our

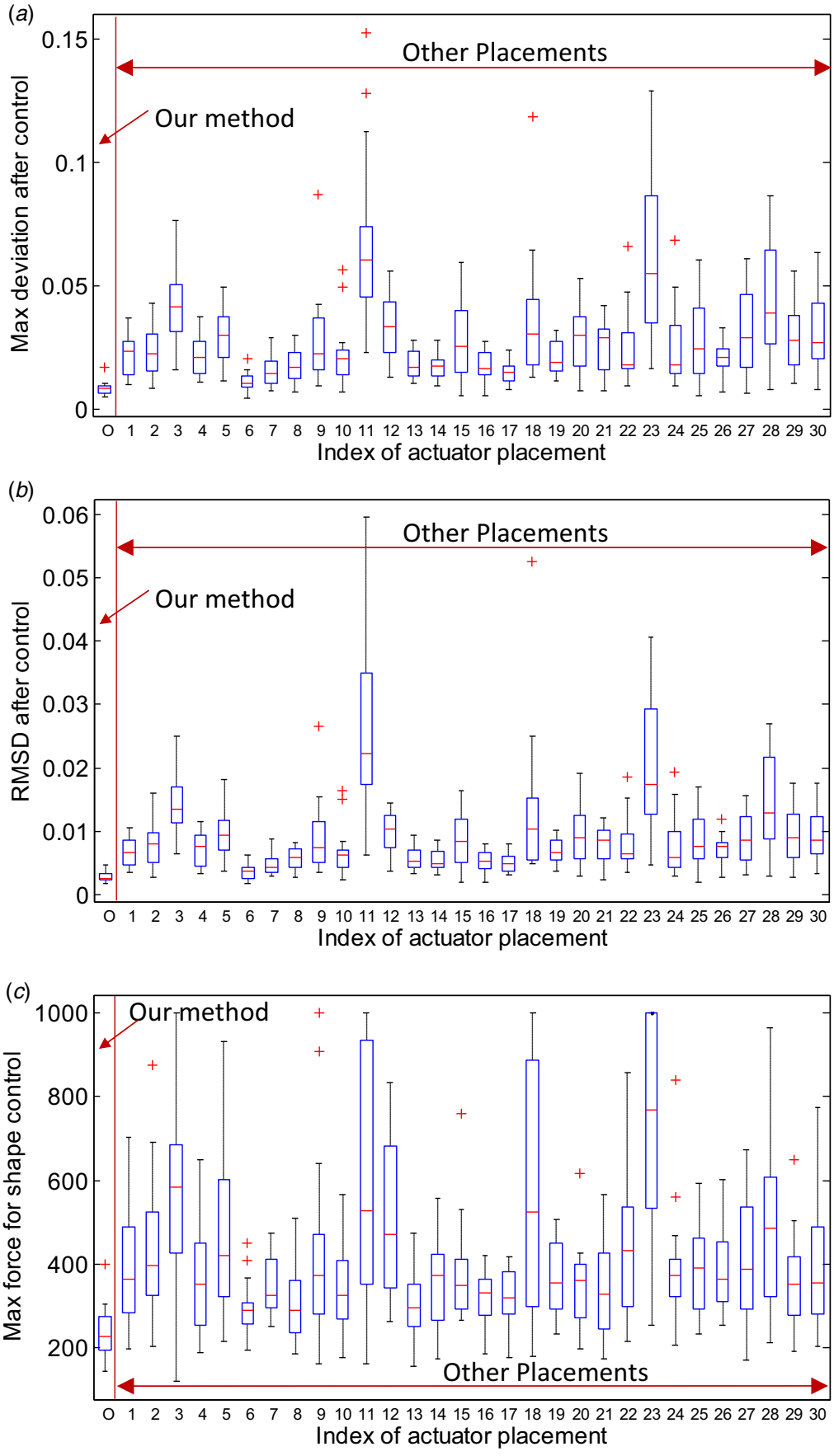

Fig. 7 Comparisons between our proposed method and the 30 fixed placements in terms of the (*a*) MD, (*b*) RMSD, and (*c*) MF

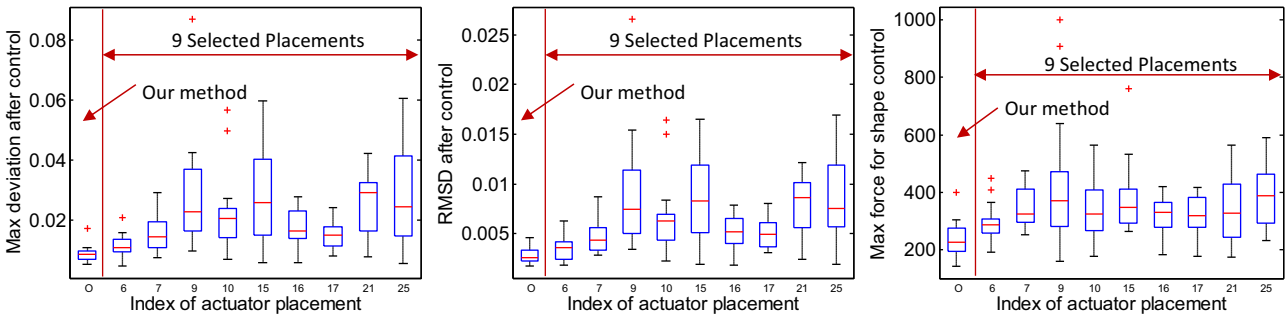

Fig. 8 Comparison results between our proposed method and nine fixed placements with the minimum MD

proposed method with the fixed actuator placement. We randomly select M actuators from m feasible locations without replacements. Thirty replications are conducted, and we obtain 30 fixed actuator placements. We compare our method with the 30 fixed actuator placements, as shown in Fig. 7. The X-axis shows the index of the actuator placement. The first index "O" denotes our method, and the rest indexes denote the 30 fixed actuator placements. For each index (e.g., each actuator placement plan), 20 testing samples are used to test our method and other placements, thereby generating a boxplot. Y-axis shows the MD, RMSD, and MF. Figure 7 shows that our method achieves the smaller adjusted shape deviations by using smaller maximum forces than the 30 fixed placements, thereby indicating that our method outperforms the fixed actuator placement.

In order to make the comparisons clearer, the authors select the actuator placement strategies that have the minimum MD from those 30 fixed placements for each testing sample. Specifically, for each one of the 20 testing samples, we select a placement that achieves the minimum MD among the original 30 fixed placements. Therefore, at most there could be 20 different fixed placements that achieve the minimum MD. In fact, we obtain only nine fixed placements, since some of them achieve the minimum MD for more than one testing samples.

Figure 8 shows the comparisons between our proposed method and the nine selected placements. The X-axis shows the index of the actuator placement. The first index "O" denotes our method, and the following denotes the indexes of the nine selected placements. Although the nine selected placements achieve the minimum MD for at least one of the 20 testing samples, these placements cannot perform well for other initial shape distortions. For comparison, our method achieves smaller adjusted shape deviations by using relatively smaller forces for different initial shape distortions, which demonstrates the effectiveness of our method more clearly.

We choose the best-fixed placement from the 30 fixed placements that achieves the minimum mean RMSD, and the comparison results are listed in Table 1. For comparison, our method uses 11.50% less max MF to achieve 16. 82% and 25.81% smaller max MD and max RMSD than the best-fixed placement, respectively. In addition, our method uses 20.54% less mean MF to achieve 22.32% and 17.65% less mean MD and mean RMSD than the best-fixed placement, respectively. Hence, our proposed method is more effective than the fixed placement method.

In order to provide the statistical evidence of the comparison, we use the paired-sample t-test to test the mean difference between the "Best" fixed placement and our method in terms of the MD, RMSD, and MF. The null hypothesis (H) is that the mean difference is zero for the MD, RMSD, and MF, respectively. If the null hypothesis is rejected at the 5% significance level, H is equal to 1. Otherwise, H is equal to 0. Table 2 lists the p-value, i.e., the probability of observing the given result, or one more extreme, by chance if the null hypothesis is true. 95% confidence interval for the true mean difference from the paired t-test is also listed in Table 2. Although the method of the "Best" fixed placement is comparable with the proposed method in terms of the mean RMSD, the mean MD and MF values are significantly larger than our method. Hence, our method is more effective than the "Best" fixed placement from 30 fixed placements.

Table 1 Comparisons between our method and the best-fixed placement from 30 fixed placements

Method	Mean MD (in.)	Mean RMSD (in.)	Mean MF (lbf)	Max MD (in.)	Max RMSD (in.)	Max MF (lbf)
Our method	0.0087	0.0028	231.2973	0.0173	0.0046	397.9796
"Best" fixed placement	0.0112	0.0034	291.0714	0.0208	0.0062	449.6754

Table 2 Results of statistical paired-sample t-test

Method	H	p-value	95% confidence interval
MD (in.)	1	0.0479	$[2.48\times10^{-5}, 0.0048]$
RMSD (in.)	0	0.0502	$[-6.13\times10^{-7}, 0.0013]$
MF (lbf)	1	1.84×10^{-5}	[37.6873, 81.8609]

4.3 Sensitivity Analysis of Part Uncertainty. In this subsection, we conduct a sensitivity analysis to see how our method performs for the fuselage with part uncertainty, which comes from the variability of raw material, such as the thickness of carbon fabrics. Without loss of generality, in this sensitivity analysis, we use 98% epoxy resin thickness of the fuselage in the studies in Secs. 4.1 and 4.2. For fair comparisons, we also use FEA simulations to generate the initial shape distortions based on the 20 testing inputs from the DOE, and 20 testing samples with part uncertainty are obtained. We test our method on the 20 testing samples with uncertainties by using the same displacement matrix $\boldsymbol{U}$ without considering part uncertainty. In Fig. 9, we list the comparison results between our proposed actuator placements and the 30 fixed actuator placements. Similarly, the X-axis shows the index of the actuator placement. The first index "O" denotes our method, and the rest indexes denote the 30 fixed actuator placements. Y-axis shows the MD, RMSD, and the MF, respectively. As shown in Fig. 9, our method achieves smaller MD, RMSD by using smaller MF. Thus, we can conclude that our method outperforms the fixed actuator placements if there is a part uncertainty.

We also compare the shape control results of the fuselages with and without part uncertainty in Fig. 10 by using our method. Small differences exist in the shape control performance between the fuselages with and without part uncertainty. In order to quantify the difference of control performance between the part with uncertainty

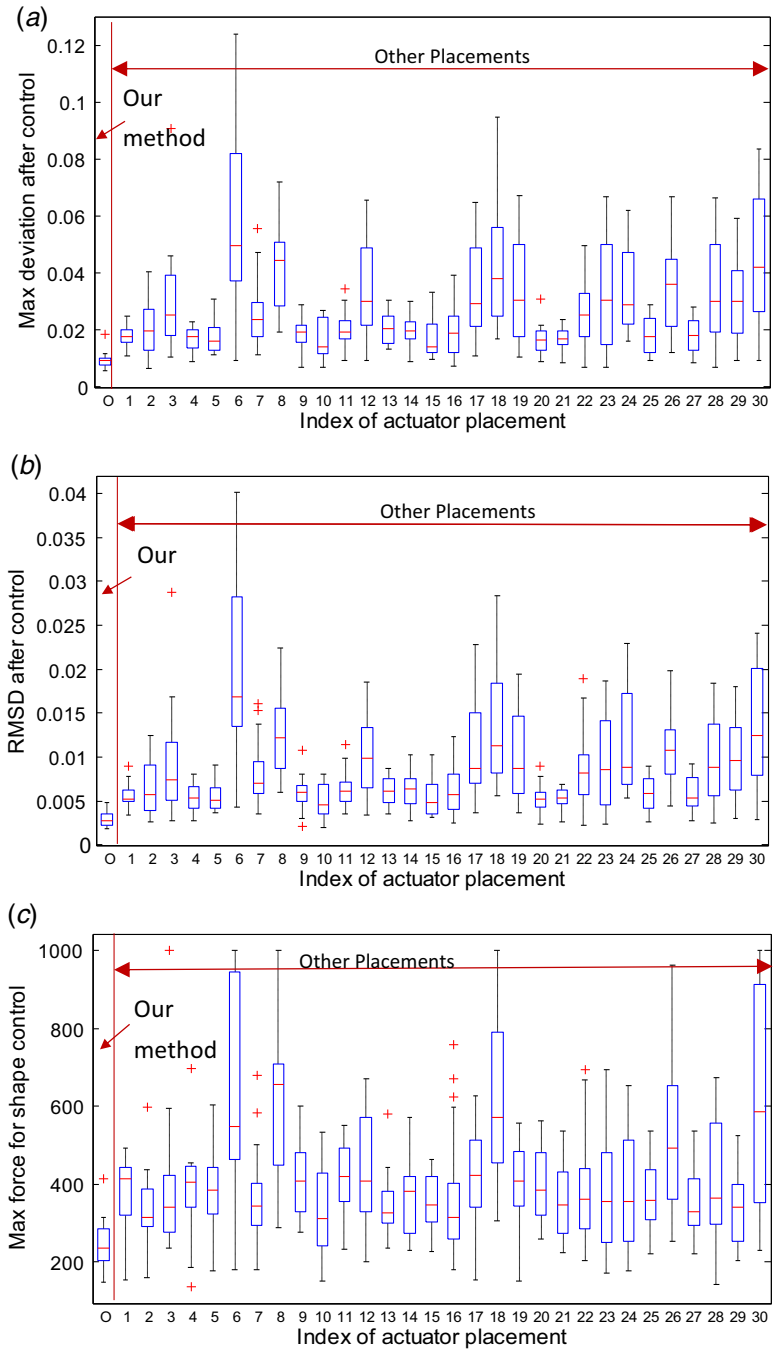

Fig. 9 The (*a*) MD, (*b*) RMSD, and (*c*) MF of our proposed actuator placements and the 30 fixed actuator placements considering part uncertainty

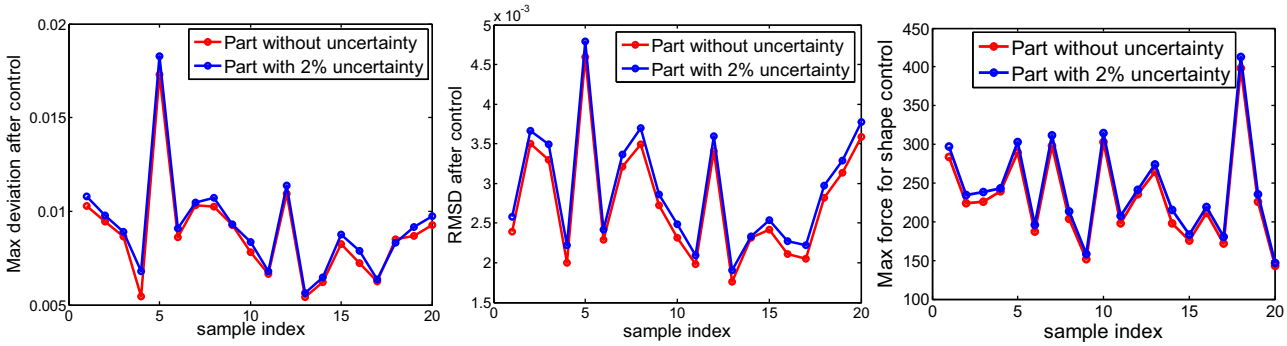

Fig. 10 Comparisons between fuselage parts with and without uncertainty in terms of the MD, RMSD, and MF

Table 3 Results of statistical paired-sample *t*-test

Evaluation index	H	*p*-value	95% confidence interval	Percentage
MD (in.)	1	2.53×10^{-5}	$[2.55 \times 10^{-4}, 5.67 \times 10^{-4}]$	[2.92%, 6.49%]
RMSD (in.)	1	3.02×10^{-9}	$[7.35 \times 10^{-7}, 1.11 \times 10^{-6}]$	[8.98%, 13.53%]
MF (lbf)	1	9.31×10^{-11}	[8.33, 11.61]	[3.60%, 5.02%]

and the part without uncertainty, the statistical paired-sample *t*-test is also used to test the mean difference of the MD, RMSD, and MF. The results are listed in Table 3. The H, *p*-value, and 95% confidence interval denote the same meaning as Table 2. As shown in Table 3, the mean MD, RMSD, and MF of the part with 2% uncertainty are significantly larger than the part without uncertainty. The reason is that the thickness of epoxy resin is thinner for the part with uncertainty, thereby leading to larger initial shape distortion under the same forces for the simulation. This fact is illustrated in Fig. 11. Hence, larger forces are needed for the part with uncertainty. Since the displacement matrix of the part without uncertainty is used for the part with uncertainty, the control performance is a little worse than the part without uncertainty. The percentages of the mean increase of the MD, RMSD, and MF are also listed in Table 3. Although introducing the uncertainty leads to the significant mean increases on the MD, RMSD, and MF, the increase percentage is very limited, thereby indicating the effectiveness of the proposed method.

We also compare the locations of actuators for the fuselages with and without part uncertainty. The actuator locations are exactly the same for the 20 testing samples. It means that the introduced uncertainty (by changing the resin epoxy thickness uniformly for the whole composite fuselage) only has an influence on the magnitude of optimal forces but not on the optimal actuator placement. The intuition behind this fact is as follows. In this simulation, we have 20 testing samples of fuselages. Given each sample of the fuselage, the force used to generate the shape distortion of the part without uncertainty is the same as the part with uncertainty. The introduced uncertainty is to change the thickness of carbon fabrics for the whole composite fuselage. In other words, the only difference of the part with uncertainty is the material thickness, so the overall shape is similar to the part without uncertainty. Figure 11 can also illustrate this fact. The actuator placement is dependent on the shape, so the introduced uncertainty only has an influence on the magnitude of optimal forces, not the optimal actuator placement.

Figure 11 shows an illustration on the actuator locations of one random sample from the 20 testing samples with and without part uncertainty. Notably, since the thickness of epoxy resin is thinner for the part with uncertainty, the initial shape distortions of the part with uncertainty is a little larger than the part without uncertainty.

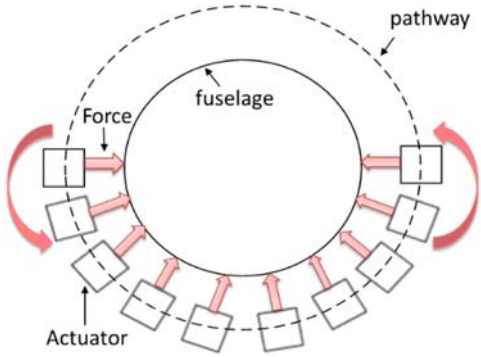

Fig. 12 The ring setup of actuators for composite fuselage shape control

Table 4 Results of shape control under different number of actuators for one sample

Binary search order/*M*	10	6	8	7
MD/in.	0.0103	0.0393	0.0216	0.0249
RMSD/in.	0.0024	0.0128	0.0062	0.0088
MF/lbf	283.5796	366.0418	266.5041	349.9775

5 Discussion

Figure 12 shows the ring setup of actuators for the new generation of actuator placement. The actuators can move along the ring pathway to get the optimal locations for fuselage shape control based on the sparse learning results. Thus, the actuators are not fixed, and the optimal actuator placement strategy is needed for fuselage shape control. This paper proposes a sparse learning model and ADMM algorithm to obtain the optimal actuator placement and the optimal forces. The methodology is validated by the aforementioned numerical studies.

Besides the optimal actuator placement given the fixed number of actuators for fuselage shape control, the proposed method can also be used to determine the minimum number of actuators given the shape control requirement. Specifically, we can use the binary search algorithm to find the minimum number of actuators so that

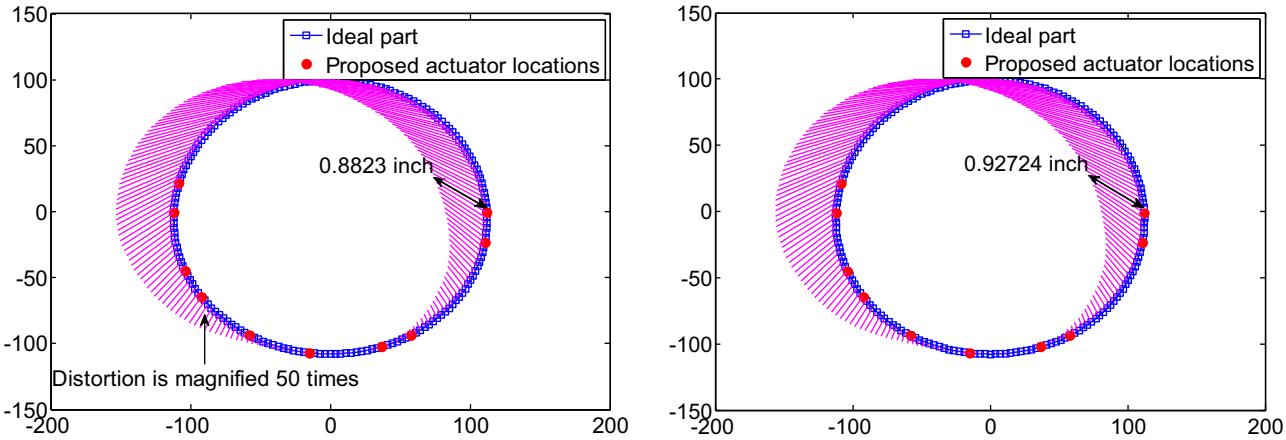

Fig. 11 Comparisons of actuator locations between the fuselages without (left) and with (right) part uncertainty on the same testing sample

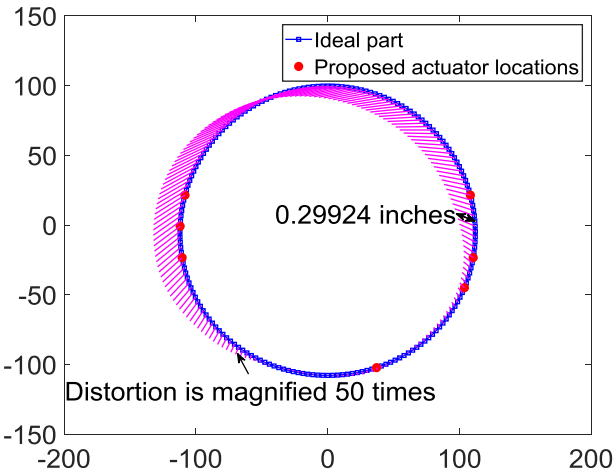

Fig. 13 The initial shape distortions of one sample and corresponding seven actuator locations

the adjusted shape deviations meet the requirements for two fuselage assembly. For example, given the engineering requirement of RMSD ≤ 0.01 in., we first try 10 actuators and find its control performance is much better than the requirements. Then, $M=6$ is tried according to the binary search algorithm. Following this procedure, the minimum number of actuators can be determined. The results of the binary search algorithm for one sample from the 20 testing samples are listed in Table 4. $M=7$ is the minimum number of actuators that meets the shape control requirements of this sample. Figure 13 shows the initial distortions of this sample and corresponding locations of seven actuators for fuselage shape control.

6 Conclusion

This paper proposes a sparse learning-based optimal actuator placement method for fuselage shape control. Due to dimensional variations of fuselages, the actuators are used for fuselage shape control in the airplane assembly process. However, how to optimally determine the locations of actuators for a given number of actuators is a challenging task due to the complexity of initial shape distortions and the structure of fuselages. To tackle these challenges, we propose a sparse learning model, which aims to select the actuator locations from all feasible locations for each initial shape of a fuselage. An efficient algorithm integrating the ADMM and the binary search is developed to estimate the model parameters.

A set of case studies show that our method achieves satisfactory performance and outperforms other fixed actuator placements for fuselage shape control in terms of the maximum of adjusted shape deviations, the root mean square of adjusted shape deviations, and the maximum force for shape control. Furthermore, a sensitivity analysis shows the performance of the proposed method is robust for the fuselage with part uncertainty.

Although our method is demonstrated for fuselage shape control, the methodology can be conceptually feasible for other large space structures, such as composite wings. However, when the linear assumption results in large prediction errors, the optimal actuator placement strategy needs further investigation. In some industrial applications such as composite fuselage shape control, experimental samples are expensive and time-consuming to obtain. The future work will be the optimization of experiment design to use the minimum of sample size to improve the predictive modeling for the automatic shape control system of the composite fuselage.

Acknowledgment

The work is partially supported by the Strategic University Partnership between the Boeing Company (Funder ID: 10.13039/100000003) and the Georgia Institute of Technology (Funder ID: 10.13039/100006778). The authors also thank Dr. Shanshan Cao for the help on the proof of Proposition 2 and Dr. Andi Wang for kind discussions.

Appendix A: Derivation of Proposition 1

Let $h(\boldsymbol{F}) = (\boldsymbol{\psi} + \boldsymbol{UF})'\boldsymbol{B}(\boldsymbol{\psi} + \boldsymbol{UF}) + \frac{\rho}{2}||\boldsymbol{F} - \boldsymbol{z}^k + \boldsymbol{u}^k||_2^2$.

To obtain the optimal F to minimize $h(\boldsymbol{F})$, we take the derivative to $\boldsymbol{F}$ on both sides, i.e., $\nabla h(\boldsymbol{F}) = 2\boldsymbol{U}'\boldsymbol{B}(\boldsymbol{\psi} + \boldsymbol{UF}) + \rho(\boldsymbol{F} - \boldsymbol{z}^k + \boldsymbol{u}^k)$.

Let $\nabla h(\boldsymbol{F}) = 0$, we get $\boldsymbol{F} = (2\boldsymbol{U}'\boldsymbol{BU} + \rho\boldsymbol{I})^{-1}(\rho\boldsymbol{z}^k - \rho\boldsymbol{u}^k - 2\boldsymbol{U}'\boldsymbol{B}\boldsymbol{\psi})$.

For formula (9), we want to obtain $\boldsymbol{F}$, which minimizes $f(\boldsymbol{F}) + \frac{\rho}{2}||\boldsymbol{F} - \boldsymbol{z}^k + \boldsymbol{u}^k||_2^2$, i.e., to minimize $(h(\boldsymbol{F}) + \chi_C)$. Due to $\chi_C = \begin{cases} \infty & \boldsymbol{F} \notin C \\ 0 & \boldsymbol{F} \in C \end{cases}$, we need to project $\boldsymbol{F}$ to C to minimize $(h(\boldsymbol{F}) + \chi_C)$. Thus,

$$\boldsymbol{F}^{k+1} := \underset{\boldsymbol{F}}{\operatorname{argmin}}\left(f(\boldsymbol{F}) + \frac{\rho}{2}||\boldsymbol{F} - \boldsymbol{z}^k + \boldsymbol{u}^k||_2^2\right)$$
$$= \prod\nolimits_C ((2\boldsymbol{U}'\boldsymbol{BU} + \rho\boldsymbol{I})^{-1}(\rho\boldsymbol{z}^k - \rho\boldsymbol{u}^k - 2\boldsymbol{U}'\boldsymbol{B}\boldsymbol{\psi}))$$

where $\prod_C$ is Euclidean projection onto the convex set $C = \{\boldsymbol{F} \in R^m: \ \boldsymbol{F}_L \preceq \boldsymbol{F} \preceq \boldsymbol{F}_Q\}$.

For formula (10), we want to obtain $\boldsymbol{z}$ to minimize $\left(g(\boldsymbol{z}) + \frac{\rho}{2}||\boldsymbol{F}^{k+1} - \boldsymbol{z} + \boldsymbol{u}^k||_2^2\right)$, which is the proximal operator of scaled function $g(\boldsymbol{z})/\rho$, i.e.,

$$\mathbf{prox}_{g/\rho}(\boldsymbol{F}^{k+1} + \boldsymbol{u}^k) = \underset{\boldsymbol{z}}{\operatorname{argmin}}\left(g(\boldsymbol{z}) + \frac{\rho}{2}||\boldsymbol{F}^{k+1} - \boldsymbol{z} + \boldsymbol{u}^k||_2^2\right)$$

Since $g(\boldsymbol{z}) = \lambda||\boldsymbol{z}||_1$, $\mathbf{prox}_{g/\rho}(\boldsymbol{F}^{k+1} + \boldsymbol{u}^k) = S_{\lambda/\rho}(\boldsymbol{F}^{k+1} + \boldsymbol{u}^k)$. The deviation of the soft thresholding operator can be referred to Ref. [26].

Appendix B: Derivation of Proposition 2

We want to prove the following:

$$\boldsymbol{F} = 0 \ \textit{if} \quad \lambda \geq \lambda_{\max} = 2||\boldsymbol{U}'\boldsymbol{B}\boldsymbol{\psi}||_\infty$$

Due to the first-order condition, we have

$$2\boldsymbol{U}'\boldsymbol{B}(\boldsymbol{\psi} + \boldsymbol{UF}) + \lambda\partial||\boldsymbol{F}||_1 = 0$$

for some subgradient $\partial||\boldsymbol{F}||_1$ of $||\boldsymbol{F}||_1$. Multiply the equation with $\boldsymbol{F}'$, we have

$$2\boldsymbol{F}'\boldsymbol{U}'\boldsymbol{B}(\boldsymbol{\psi} + \boldsymbol{UF}) + \lambda\langle \boldsymbol{F}, \partial||\boldsymbol{F}||_1\rangle = 0$$

Since $\boldsymbol{B}$ is a weight matrix, which is a positive diagonal matrix, $\boldsymbol{U}'\boldsymbol{BU}$ is symmetric positive definite. Thus, we have

$$0 \leq 2\boldsymbol{F}'\boldsymbol{U}'\boldsymbol{BUF} = -2\boldsymbol{F}'\boldsymbol{U}'\boldsymbol{B}\boldsymbol{\psi} - \lambda\langle \boldsymbol{F}, \partial||\boldsymbol{F}||_1\rangle \qquad \text{(B1)}$$

On the other hand, note $\partial||\boldsymbol{F}_i||_1 = \begin{cases} 1, & \boldsymbol{F}_i > 0 \\ -1, & \boldsymbol{F}_i < 0 \\ [-1,\ 1], & \boldsymbol{F}_i = 0 \end{cases}$. Since $\lambda \geq 2||\boldsymbol{U}'\boldsymbol{B}\boldsymbol{\psi}||_\infty$, for $i \in S = \{i: \boldsymbol{F}_i \neq 0\}$, we have

$$\operatorname{sign}(2\boldsymbol{U}'\boldsymbol{B}\boldsymbol{\psi} + \lambda\partial||\boldsymbol{F}_1||)_i = \operatorname{sign}(\boldsymbol{F}_i),$$

where $\operatorname{sign}(x) = 1$ for $x > 0$ and -1 otherwise. It can be easily checked that

$$2\boldsymbol{F}'\boldsymbol{U}'\boldsymbol{B}\boldsymbol{\psi} + \lambda\langle \boldsymbol{F}, \partial||\boldsymbol{F}||_1\rangle = \mathbf{F}_S'(2\boldsymbol{U}'\boldsymbol{B}\boldsymbol{\psi} + \lambda\partial||\boldsymbol{F}||_1)_S$$
$$+ \boldsymbol{F}_{S^c}'(2\boldsymbol{U}'\boldsymbol{B}\boldsymbol{\psi} + \lambda\partial||\boldsymbol{F}||_1)_{S^c} = \boldsymbol{F}_S'(2\boldsymbol{U}'\boldsymbol{B}\boldsymbol{\psi} + \lambda\partial||\boldsymbol{F}||_1)_S > 0$$

This shows the contradiction in Eq. (B1), which completes the proof.

References

[1] Chawla, K. K., 2012, *Composite Materials: Science and Engineering*, Springer Science & Business Media, New York. Chap. 5.

[2] Gates, D., 2007, "Boeing Finds 787 Pieces Aren't Quite A Perfect Fit," Seattle Times aerospace report, Seattle Times, http://www.seattletimes.com/business/boeing-finds-787-pieces-arent-quite-a-perfect-fit/.
[3] Wen, Y., Yue, X., Hunt, J. H., and Shi, J., 2018, "Feasibility Analysis of Composite Fuselage Shape Control Via Finite Element Analysis," J. Manuf. Syst., **46**, pp. 272–281.
[4] Yue, X., Wen, Y., Hunt, J. H., and Shi, J., 2018, "Surrogate Model-Based Control Considering Uncertainties for Composite Fuselage Assembly. ASME Transactions," ASME J. Manuf. Sci. Eng., **140**(4), p. 041017.
[5] Morris, K., and Yang, S., 2015, "Comparison of Actuator Placement Criteria for Control of Structures," J. Sound Vib., **353**, pp. 1–18.
[6] Chee, C., Tong, L., and Steven, G. P., 2001, "Static Shape Control of Composite Plates Using a Curvature–Displacement Based Algorithm," Int. J. Solids Struct., **38**(36–37), pp. 6381–6403.
[7] Haftka, R. T., and Adelman, H. M., 1985, "An Analytical Investigation of Shape Control of Large Space Structures by Applied Temperatures," AIAA J., **23**(3), pp. 450–457.
[8] Burdisso, R. A., and Haftka, R. T., 1990, "Statistical Analysis of Static Shape Control in Space Structures," AIAA J., **28**(8), pp. 1504–1508.
[9] Hakim, S., and Fuchs, M., 1995, "Optimal Actuator Placement with Minimum Worst Case Distortion Criterion (Space Truss Structures)," 36th Structures, Structural Dynamics and Materials Conference, New Orleans, LA, Apr. 10–13.
[10] Haftka, R. T., and Adelman, H. M., 1985, "Selection of Actuator Locations for Static Shape Control of Large Space Structures by Heuristic Integer Programing," Adv. Trends Struct Dyn., **20**(1–3), pp. 575–582.
[11] Burdisso, R. A., and Haftka, R. T., 1989, "Optimal Location of Actuators for Correcting Distortions in Large Truss Structures," AIAA J., **27**(10), pp. 1406–1411.
[12] Ponslet, E., Haftka, R., and Cudney, H., 1993, "Optimal Placement of Tuning Masses on Truss Structures by Genetic Algorithms," 34th Structures, Structural Dynamics and Materials Conference, La Jolla, CA, Apr. 19–22.
[13] Jiao, Y., and Djurdjanovic, D., 2008, "Allocation of Flexible Tooling for Optimal Stochastic Multistation Manufacturing Process Quality Control," ASME 2008 International Manufacturing Science and Engineering Conference Collocated with the 3rd JSME/ASME International Conference on Materials and Processing, Evanston, IL, Oct. 7–10.
[14] Furuya, H., and Haftka, R. T., 1995, "Placing Actuators on Space Structures by Genetic Algorithms and Effectiveness Indices," Struct. Optim., **9**(2), pp. 69–75.
[15] Jiao, Y., and Djurdjanovic, D., 2010, "Joint Allocation of Measurement Points and Controllable Tooling Machines in Multistage Manufacturing Processes," IIE Trans., **42**(10), pp. 703–720.
[16] Wen, Y., Yue, X., Hunt, J. H., and Shi, J., 2019, "Virtual Assembly and Residual Stress Analysis for Composite Fuselage Assembly Process," J. Manuf. Syst., **52**, pp. 55–62.
[17] Natarajan, B. K., 1995, "Sparse Approximate Solutions to Linear Systems," SIAM J. Comput., **24**(2), pp. 227–234.
[18] Amaldi, E., and Kann, V., 1998, "On The Approximability of Minimizing Nonzero Variables or Unsatisfied Relations in Linear Systems," Theor. Comput. Sci., **209**(1–2), pp. 237–260.
[19] Donoho, D. L., 2006, "For Most Large Underdetermined Systems of Linear Equations the Minimal ℓ1-Norm Solution is Also the Sparsest Solution," Commun. Pure Appl. Math., **59**(6), pp. 797–829.
[20] Dowling, N. E., 2012, *Mechanical Behavior of Materials: Engineering Methods for Deformation, Fracture, and Fatigue*, Prentice Hall, Upper Saddle River, NJ.
[21] Friedman, J., Hastie, T., and Tibshirani, R., 2001, *The Elements of Statistical Learning*, Springer Science&Business Media, New York.
[22] Boyd, S., and Vandenberghe, L., 2004, *Convex Optimization*, Cambridge University Press, New York.
[23] Boyd, S., Parikh, N., Chu, E., Peleato, B., and Eckstein, J., 2011, "Distributed Optimization and Statistical Learning via the Alternating Direction Method of Multipliers," Found. Trends Mach Learn., **3**(1), pp. 1–122.
[24] Demmel, J. W., 1997, *Applied Numerical Linear Algebra* (Vol. 56), SIAM, Philadelphia, PA.
[25] Morris, M. D., and Mitchell, T. J., 1995, "Exploratory Designs for Computational Experiments," J. Stat. Plann. Inference, **43**(3), pp. 381–402.
[26] Parikh, N., and Boyd, S., 2014, "Proximal Algorithms," Found Trends Optim., **1**(3), pp. 127–239.